The effect of linear shear current on head-on collision of solitons

Li, Mingjie; Zhao, Binbin ; Duan, Wenyang; Ertekin, R. Cengiz; Hayatdavoodi, Masoud

Published in:
Physics of Fluids

DOI:
10.1063/5.0151627

Publication date:
2023

Document Version
Peer reviewed version

The effect of linear shear current on head-on collision of solitons

Mingjie Li (李明杰),[1] Binbin Zhao (赵彬彬),[1, a)] Wenyang Duan (段文洋),[1] R. Cengiz Ertekin,[1, 2] and Masoud Hayatdavoodi[1, 3]

[1)]*College of Shipbuilding Engineering, Harbin Engineering University, 150001 Harbin, China*

[2)]*Department of Ocean and Resources Engineering, University of Hawai'i, Honolulu, HI 96822, USA*

[3)]*Civil Engineering Department, School of Science and Engineering, University of Dundee, Dundee, DD1 4HN, UK*

(Dated: 17 May 2023)

Head-on collision of two solitary waves in the presence of linear shear currents is studied by use of the High-Level Green-Naghdi (HLGN) theory. The finite difference method is used to solve the HLGN model in the time-domain simulation. The initial values are obtained by the steady solution of solitary waves in the presence of linear shear currents. Shear currents with different velocities are considered to assess their effect on the solitary-wave collision. Three aspects of the head-on collision process in the presence of shear current are studied, namely the wave elevation, velocity field and particle trajectory. Results show that the background linear shear current significantly affects the wave elevation, velocity field and particle trajectory during the head-on collision. It is observed that in the presence of the current, the wave elevation is narrower near the maximum surface displacement, and is wider near the still water level. It is also shown that near the seafloor, the horizontal velocity is opposite of the current direction, while it is following the current direction near the free surface. The opposite shear current results in formation of a vortex in the fluid field. At the point of the collision, the vortex appears at a lower vertical position and shifts upstream of the current direction. Following the particle trajectories in the presence of the shear current, it is observed that the particles do not return to their initial positions after the head-on collisions, and the loop motions of the particles become smaller with larger current velocities.

I. INTRODUCTION

The solitary wave has received significant attention from the research community due to its interesting characteristics and applications. Solitary waves have applications in water waves, physics of optics, electricity and medicine. Here, our primary attention is on the water-wave applications.

The KdV equation[1] has been widely used to study solitary waves. The KdV theory uses the first-order approximation and it is mostly applicable to small-amplitude solitary waves. Alternative solutions are required when large-amplitude solitary waves are of interest, such as by solving Euler's equations as in Dutykh and Clamond[2] and by solving the High-Level Green-Naghdi (HLGN, hereafter) equations by Zhao et al.[3] and solving the Irrotational Green-Naghdi (IGN) equations by Duan et al.[4]. Hunter and Vanden-Broeck[5] presented a method based on series truncation to calculate the highest solitary wave in which the ratio of the wave amplitude to the water depth was 0.83322. Wang and Liu[6] presented experimental data for surface elevation and particle velocity for the nonlinearity parameter $H/d \leq 0.6$. They assessed the accuracy of the numerical and approximate analytical solutions using these experimental data.

Current also plays an important role in the ocean dynamics. Presence of the background current and vorticity change the properties and behaviour of water waves. Freeman and Johnson[7] derived a modified KdV equation for waves on shear currents. Dalrymple[8] used the series expansion of the stream function formulation to study water waves propagating on currents with constant vorticity. They found that the current changes the wavelength and the kinematics under the wave. Meanwhile, the background current significantly affected the wave profile. The boundary integral equation method was used to obtain solutions of periodic waves in finite water depth with the constant vorticity by Teles Da Silva and Peregrine[9]. Swan[10] provided experimental data of the surface elevation and horizontal velocity for regular waves on currents with constant vorticity. Results showed that strongly opposing sheared current modify the wave induced flow field and increase the amplitude of the oscillatory motion significantly. Vanden-Broeck[11] obtained the solitary wave solutions in finite water depth with constant vorticity using the boundary integral equation method. The branches of solutions and limiting configurations were studied. Under the long-wave approximation, Choi[12] obtained the wave profiles and streamlines of solitary waves in the presence of a linear shear current by use of the asymptotic method. Choi[12] found out that the solitary-wave profile is narrower when the wave and the background current propagate in the same direction. The opposite occurs when the solitary wave propagates against the current direction. Constantin et al.[13] proved that the governing equations have a nearly-Hamiltonian structure for water waves with constant non-zero vorticity, which changes to Hamiltonian for steady waves. Pak and Chow[14] used the perturbation method to obtain the third-order solution of a solitary wave in the presence of a linear shear current and second-order solutions for other current-type cases. They compared the wave profile and speed for a solitary wave in different-type shear currents. Guyenne[15] used the High-Order Spectral (HOS) method to numerically simulate a solitary wave propagating

[a)]Electronic mail: zhaobinbin@hrbeu.edu.cn

in the background linear shear current in the time domain, where the computational errors on energy, impulse and volume of the numerical tank are shown to affect the accuracy of the simulations. Duan et al.[16] used the HLGN model to obtain the steady solution of solitary waves in the presence of linear shear currents, including the wave profile, wave speed and velocity field. Later, Wang et al.[17] used the HLGN model to study the vorticity field and particle trajectories of a solitary wave in the presence of a nonlinear shear current. Gao et al.[18] developed the time-dependent conformal mapping techniques to study hydroelastic solitary waves in the presence of constant vorticity. Dynamics and stability of the generalized solitary waves are examined. The nonlinear Schrödinger equation was used to describe waves slowly modulated by the linear shear current by Li et al.[19]. The current effect on modulational instability and wave steepness was studied. Later, Li et al.[20] and Li et al.[21] derived the nonlinear Schrödinger equation to study the interfacial waves modulated by the linear shear current. Wang et al.[22] studied the flow dynamics beneath flexural-gravity solitary waves by solving the fully nonlinear equations. It was found that there was net vertical transport of particles beneath some solitary waves due to wave-current interactions.

Wave-wave interaction is an interesting topic to water-wave mechanics and coastal-engineering applications. Solitary waves propagating in the opposite directions pass through each other and almost keep their identity intact after the collision. Some laboratory experiments have been conducted on the head-on collision of solitary waves without a background current. Maxworthy[23] confirmed that the maximum surface displacement, observed at the collision point, was greater than the sum of the amplitudes of two solitary waves during their head-on collisions. Hammack et al.[24] provided high resolution measurements of the surface elevation at different moments during the two solitary-wave head-on collisions. Besides the surface elevation, Chen and Yeh[25] measured the phase shift, collision runup and rundown processes and the energy loss by the collision. Later, Chen et al.[26] measured the velocity and acceleration field and vorticity during the solitary-wave head-on collisions in laboratory. Umeyama et al.[27] experimentally studied the particle trajectories of head-on collision of two equal solitary waves. Results showed that most particles returned to their initial position, but not all. Later, Umeyama[28] extended the laboratory experiments to unequal amplitudes cases. The particles returned toward their initial positions after the collision with slightly diverted paths comparing with those before the collision. The gap between the two paths become more significant with larger difference of the two wave heights.

Solitary-wave head-on collisions without background current has been studied by numerical and theoretical approaches. Byatt-Smith[29] derived an integral equation for unsteady surface waves, and showed that the maximum surface displacement during head-on collisions of two solitary waves with equal amplitude was more than twice the initial solitary-wave amplitudes. Su and Mirie[30] obtained a third-order solution of the head-on collision of two solitary waves with arbitrary amplitudes based on the perturbation method. They gave the formulas to calculate the maximum surface displacement and the phase shifts during the collisions. In a later study, Mirie and Su[31] considered the following wave trains (waves propagating in the same directions as the solitary wave) and found out that the following wave trains took the energy of solitary waves and caused the wave-amplitude reduction after collisions. Ertekin and Wehausen[32] simulated the collision of two solitary waves by use of the Level I Green-Naghdi equations and showed the results of colliding processes, maximum run-up and phase shift. Craig et al.[33] performed a numerical analysis to solve Euler's equations by use of a pseudo-spectral method for head-on collisions. They presented the relationship between the amplitude change of solitary waves and the energy carried away from the interaction. Chambarel et al.[34] studied the head-on collision of two solitary waves by use of the boundary integral equation. They investigated the maximum run-up, phase shift and acceleration field. Ertekin et al.[35] used the Irrotational Green-Naghdi (IGN) equations with different levels and the original Green-Naghdi equations (Level I) to study the collision of two solitary waves. They determined that the IGN Level III model was the converged level of the IGN equations, which can be used to simulate the solitary-wave collision in their test cases. Tong et al.[36] created a numerical wave tank based on the Harmonic Polynomial Cell (HPC) method. Their numerical results on wave elevation of the two solitary-wave collisions were in agreement with the laboratory measurements of Chen and Yeh[25]. Zhang et al.[37] used a two-phase flow model based on Adaptive Mesh Refinement grid to study the effect of a submerged bottom-mounted barrier on the head-on collision of two solitary waves. The submerged bottom-mounted barrier affected the wave amplitudes and resulted in the vortex shedding. Karakoc et al.[38] implemented a sextic B-spline functions Subdomain approach to study the nonlinear generalized equal width equation with some fixed choices initial and boundary conditions. The collision of two solitary waves was simulated to demonstrate the accuracy and efficiency of the method. Choi[39] studied a strongly nonlinear long wave system expanded by a single small parameter, the ratio of the water depth to the characteristic wavelength. The numerical results on the head-on collision between two counter-propagating solitary waves showed good agreement with the laboratory measurements of Chen and Yeh[25].

Very few studies focus on the solitary-wave collision in the presence of a current. Umeyama[40] conducted laboratory experiments on the rear-end collisions of two solitary waves in the presence of a uniform current. The experimental data showed that the uniform current without vorticity had a little effect on the wave surface, but affected the velocity field significantly.

Background current is usually present in the oceans, and are commonly nonuniform[9]. As mentioned before, many studies pointed out that the linear shear current changes the properties of solitary waves significantly. The head-on collision of two solitary waves without currents were also studied widely. However, the linear shear current effect has not been considered on the head-on collision of the two solitary waves. This study aims to address such gaps. Thus, the motivation of

this work is to study the effect of the linear shear current on the head-on collision of two solitary waves. Here, we use the HLGN equations to study this problem, including the wave elevation, velocity field and particle trajectory.

This paper is organized as follows. In Section II, the HLGN theory is introduced. Section III presents the initial conditions and validates their accuracy. In Section IV, numerical cases of the head-on collision of two solitary waves in the presence of a linear shear current are presented. Conclusions are reached in Section V.

II. HLGN THEORY

In this study, the fluid is assumed as incompressible and inviscid. The flow can be rotational in general. The origin of the two-dimensional coordinate system is located at the still-water level (SWL, hereafter), x (positive to the right) is the horizontal axis and z (positive up) is the vertical axis. $z=\eta(x,t)$ represents the free surface and $z=-d$ represents the bottom, where d is the constant water depth and t is time.

The mass conservation equation is written as

$$\frac{\partial u}{\partial x}+\frac{\partial w}{\partial z}=0, \tag{1}$$

where u and w are the horizontal and vertical velocity components, respectively.

The momentum conservation equations are written as

$$\frac{\partial u}{\partial t}+u\frac{\partial u}{\partial x}+w\frac{\partial u}{\partial z}=-\frac{1}{\rho}\frac{\partial p}{\partial x}, \tag{2a}$$

$$\frac{\partial w}{\partial t}+u\frac{\partial w}{\partial x}+w\frac{\partial w}{\partial z}=-\frac{1}{\rho}\frac{\partial p}{\partial z}-g, \tag{2b}$$

where ρ is the constant fluid-mass density, p is pressure and g is gravitational acceleration. The free-surface pressure is the atmospheric pressure that can be treated as zero (without loss of generality).

The boundary kinematic conditions of the free surface and the flat bottom are written as

$$w=\frac{\partial \eta}{\partial t}+u\frac{\partial \eta}{\partial x} \qquad (z=\eta(x,t)), \tag{3a}$$

$$w=0 \qquad (z=-d). \tag{3b}$$

In the HLGN model, the velocity field is assumed as

$$u(x,z,t)=\sum_{n=0}^{K-1}u_n(x,t)z^n, \tag{4a}$$

$$w(x,z,t)=\sum_{n=0}^{K}w_n(x,t)z^n, \tag{4b}$$

where u_n and w_n are the unknown velocity coefficients that are part of the solution. K is the level of the HLGN model (e.g., HLGN-4 model when $K=4$), see Zhao et al.[41].

Substituting Eq. (4) into Eq. (1) gives

$$w_n=-\frac{1}{n}\frac{\partial u_{n-1}}{\partial x} \qquad (n=1,2,\ldots,K). \tag{5}$$

Substituting Eq. (4) into Eq. (2), after multiplying each term by z^n and integrating from bottom $-d$ to free surface η along the vertical direction and substituting p with the integrated pressure, we obtain

$$\frac{\partial}{\partial x}\left(G_n+gS1_n\right)+nE_{n-1}-(-d)^n\frac{\partial}{\partial x}\left(G_0+gS1_0\right)=0 \qquad (n=1,2,\cdots,K), \tag{6}$$

where

$$G_n=\sum_{m=0}^{K}\left(\frac{\partial w_m}{\partial t}S2_{mn}+\frac{\partial w_m}{\partial x}Q_{mn}+w_mH_{mn}\right), \tag{7a}$$

$$E_n=\sum_{m=0}^{K}\left(\frac{\partial u_m}{\partial t}S2_{mn}+\frac{\partial u_m}{\partial x}Q_{mn}+u_mH_{mn}\right), \tag{7b}$$

$$Q_{mn}=\sum_{r=0}^{K}u_rS3_{mrn}, \quad H_{mn}=\sum_{r=0}^{K}w_rS4_{mrn}, \tag{7c}$$

$$S1_n=\int_{-d}^{\eta}z^n\mathrm{d}z, \quad S2_{mn}=\int_{-d}^{\eta}z^{m+n}\mathrm{d}z, \tag{7d}$$

$$S3_{mrn}=\int_{-d}^{\eta}z^{m+r+n}\mathrm{d}z, \quad S4_{mrn}=m\int_{-d}^{\eta}z^{m+r+n-1}\mathrm{d}z, \tag{7e}$$

$$u_K=0. \tag{7f}$$

Substituting Eq. (4) into Eq. (3), we have

$$\frac{\partial \eta}{\partial t}=\sum_{n=0}^{K}\eta^n\left(w_n-\frac{\partial \eta}{\partial x}u_n\right), \tag{8a}$$

$$w_0=-\sum_{n=1}^{K}w_n(-d)^n. \tag{8b}$$

We use Eq. (5) and Eq. (8b) to eliminate the vertical-velocity component w_n. Hence, there are $K+1$ number of unknowns, namely η and u_n $(n=0,1,\cdots,K-1)$. On the other hand, Eq. (6) and Eq. (8a) provide the $K+1$ equations. This system of equations is closed and solvable. The finite difference method is used to solve the HLGN model in the time domain simulation. Details of the algorithm used to solve the HLGN model can be found in Zhao et al.[41].

III. INITIAL CONDITIONS

In this section, we present two kinds of initial conditions of the HLGN model, including:

1) single solitary-wave propagation in the presence of a linear shear current;

2) head-on collision of two solitary waves in the presence of a linear shear current.

The following numerical tests are also performed to validate the accuracy of the initial conditions in this section.

A. Single solitary-wave propagation in the presence of a linear shear current

For the first kind of initial conditions, we consider the single solitary-wave propagation in the presence of a linear

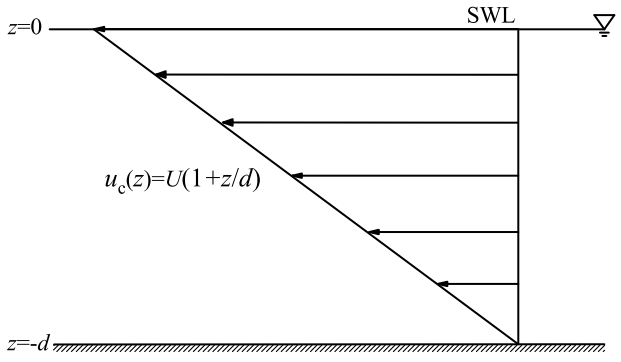

FIG. 1. Sketch of the linear shear current.

shear current. The linear shear-current type is described as $u_c(z) = U(1+z/d)$ as shown in Fig. 1, where U is the current speed at the SWL. Related parameters of the cases are shown in Table I, where H is the solitary wave amplitude and $c_0 = \sqrt{gd}$.

TABLE I. Parameters of the two cases of single solitary-wave propagation in a linear shear current $u_c(z) = U(1+z/d)$.

Case	H/d	U/c_0	Solitary-wave propagation direction
1	0.3	-0.5	left to right (Opposite)
2	0.3	-0.5	right to left (Following)

The initial values are obtained by the steady solution of solitary waves in the presence of a linear shear current, see Duan et al.[16], including the wave profile $\eta'(X)$, velocity coefficients $u'_n(X)(n = 0,\cdots,K-1)$ and wave speed c', where the primes in the variables represent the initial values of the solitary waves in the computational domain. We set the initial solitary-wave solutions in the region $x_1 \le x \le x_2$. The sketch of Case 1 is shown in Fig. 2. The linear shear current is set everywhere, for $x < x_1$ and $x > x_2$.

As shown in Fig. 2, when we consider the single solitary wave propagating from left to right (i.e. propagating in the opposing shear current, Case 1), initial values in the region $x_1 \le x \le x_2$ are given by:

$$\eta(x;t=0) = \eta'(X), \tag{9a}$$
$$u_n(x;t=0) = u'_n(X) \ \ (n = 0,\cdots,K-1), \tag{9b}$$
$$\frac{\partial \eta(x;t=0)}{\partial t} = -c'\frac{\partial \eta'(X)}{\partial X}, \tag{9c}$$

where $X = x - x_0$, x_0 is the initial position of the solitary-wave crest in the global coordinate system oxz.

When we consider the single solitary wave propagating from right to left (i.e. propagating in the following shear current, Case 2), the initial values in the region $x_1 \le x \le x_2$ are given by:

$$\eta(x;t=0) = \eta'(X), \tag{10a}$$
$$u_n(x;t=0) = -u'_n(X) \ \ (n = 0,\cdots,K-1), \tag{10b}$$
$$\frac{\partial \eta(x;t=0)}{\partial t} = c'\frac{\partial \eta'(X)}{\partial X}. \tag{10c}$$

After comparing results of the HLGN model for different level K (given in Eq. (4)), we have determined that the HLGN-5 model provides the converged HLGN results for this case. For the details of the convergence tests of the HLGN model, we refer the reader to Zhao et al.[41]. Figures 3(a) and 3(b) show the profiles of the solitary wave during its propagation at different times for the opposing-current case (Case 1) and the following-current case (Case 2), respectively, where we recenter all the wave crests at $x/d = 0$. The initial values are obtained by the steady solution of solitary waves in the presence of a linear shear current in Duan et al.[16]. We observe that during the solitary-wave propagation in the linear shear current, the wave profiles do not change, both for the opposing-current case and following-current case. It is demonstrated that initial conditions of the single solitary-wave propagation in the presence of a linear shear current are accurate.

B. Head-on collision of two solitary waves in the presence of a linear shear current

We also consider the head-on collision of two solitary waves in the presence of a linear shear current. Initial conditions are shown in Fig. 4. The solution of solitary wave propagating from left to right is set in region $x_1 \le x \le x_2$, and the solution of solitary wave propagating from right to left is set in region $x_3 \le x \le x_4$. $c_1{}'$ and $c_2{}'$ are speeds of the right-going solitary wave and the left-going solitary wave, respectively. The linear shear current is set everywhere outside these regions.

To validate the accuracy of initial conditions, we study the head-on collision of two solitary waves in the absence of current numerically by use of the HLGN model, and compare our results with the results of the Harmonic Polynomial Cell (HPC) method of Tong et al.[36] and the experimental data of Chen and Yeh[25] (further discussion on head-on collision of two solitary waves in the presence of a linear shear current will be provided in the next section). Parameters of this case are shown in Table II, where $(H/d)_L$ is the amplitude of the left solitary wave propagating to the right, and $(H/d)_R$ is the amplitude of the right solitary wave propagating to the left. Note that in this case, there is no current, i.e. $U/c_0 = 0$. Initial amplitudes of the two solitary waves we select are $(H/d)_L = 0.4014$ and $(H/d)_R = 0.3887$, which are captured from Fig. 4(a) of Chen and Yeh[25]. In this case, we have determined that the HLGN-4 model provides the converged HLGN results for this case.

The comparison between the HLGN results, HPC results of Tong et al.[36] and the experimental data of Chen and Yeh[25] of the surface elevation snapshots at different times is shown in Fig. 5. We note that $t\sqrt{g/d} = 0$ is taken as the moment when the maximum surface displacement occurs. From Fig. 5, we

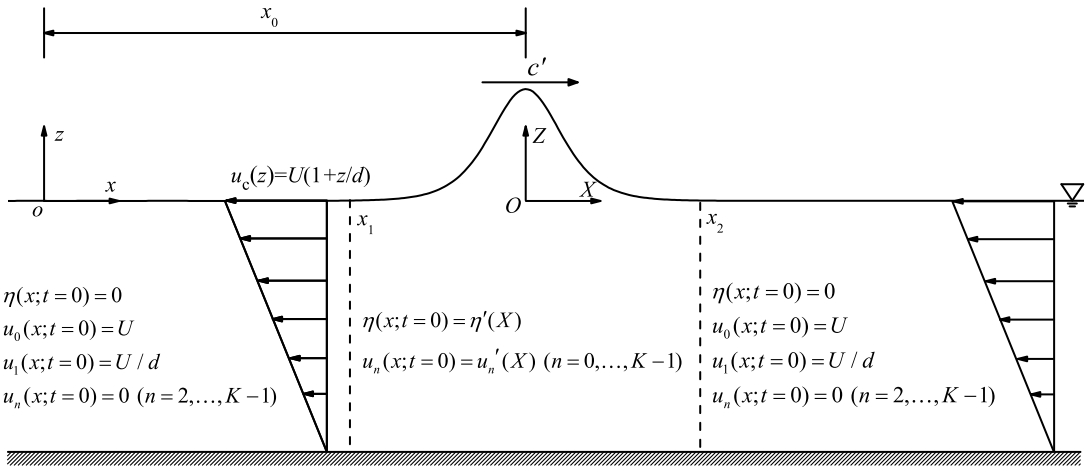

FIG. 2. Initial conditions of Case 1 for the single solitary-wave propagation in the presence of a linear shear current.

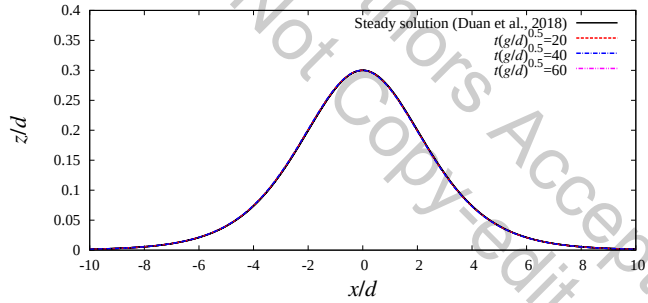

(a) Solitary wave propagating from left to right, Case 1.

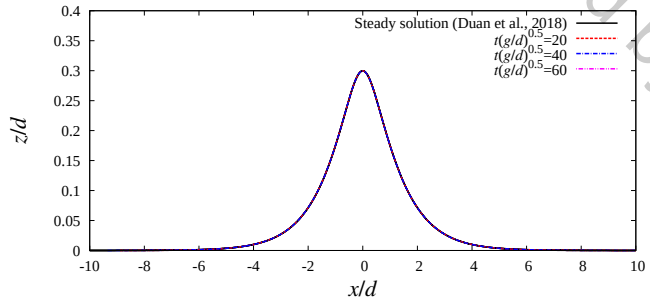

(b) Solitary wave propagating from right to left, Case 2.

FIG. 3. Profiles of the solitary wave propagating in the linear shear current at different times, $U/c_0 = -0.5, H/d = 0.3$.

observe that the HLGN results and the HPC results show very good agreement, and they both match the experimental data well. It is demonstrated that initial conditions to simulate the head-on collision of the two solitary waves in the absence of a current are accurate.

Based on the cases discussed in this section, it is shown that initial conditions are set properly to simulate the single solitary-wave propagation in the presence of a linear shear current, and the head-on collision of the two solitary waves in the absence of current by the HLGN model. Next, the HLGN model will be used to study the head-on collision of two solitary waves in the presence of a linear shear current.

TABLE II. Parameters of the head-on collision of the two solitary waves in the absence of current.

Case	$(H/d)_L$	$(H/d)_R$	U/c_0
3	0.4014	0.3887	0

IV. RESULTS AND DISCUSSION

In this section, the head-on collision of two solitary waves in the presence of a linear shear current is studied by use of the HLGN model discussed in the previous sections. Results presented include the surface elevation, velocity field and particle trajectory. The linear shear current is described as $u_c(z) = U(1+z/d)$ and is shown in Fig. 1. In this study, we consider two solitary waves with the same amplitude $H/d = 0.3$. Parameters of the cases considered here are given in Table III.

TABLE III. Parameters of the head-on collision of the two solitary waves in the presence of a linear shear current, $u_c(z) = U(1+z/d)$.

Case	$(H/d)_L$	$(H/d)_R$	U/c_0
4	0.3	0.3	0
5	0.3	0.3	-0.1
6	0.3	0.3	-0.3
7	0.3	0.3	-0.5

Initially, we place the two steady solitary waves in a linear shear current in the computational domain. The length of the computational domain is $x/d = 150$. The peak of the left

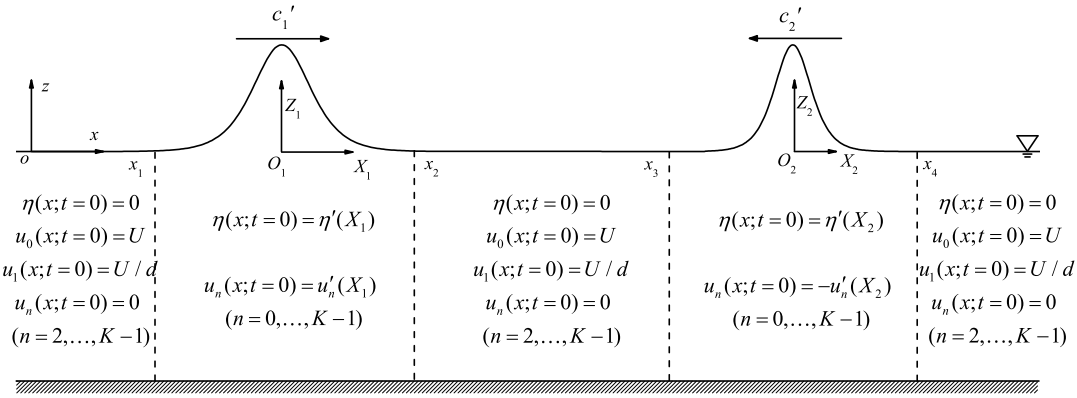

FIG. 4. Initial conditions for the head-on collision of two solitary waves in the presence of a linear shear current.

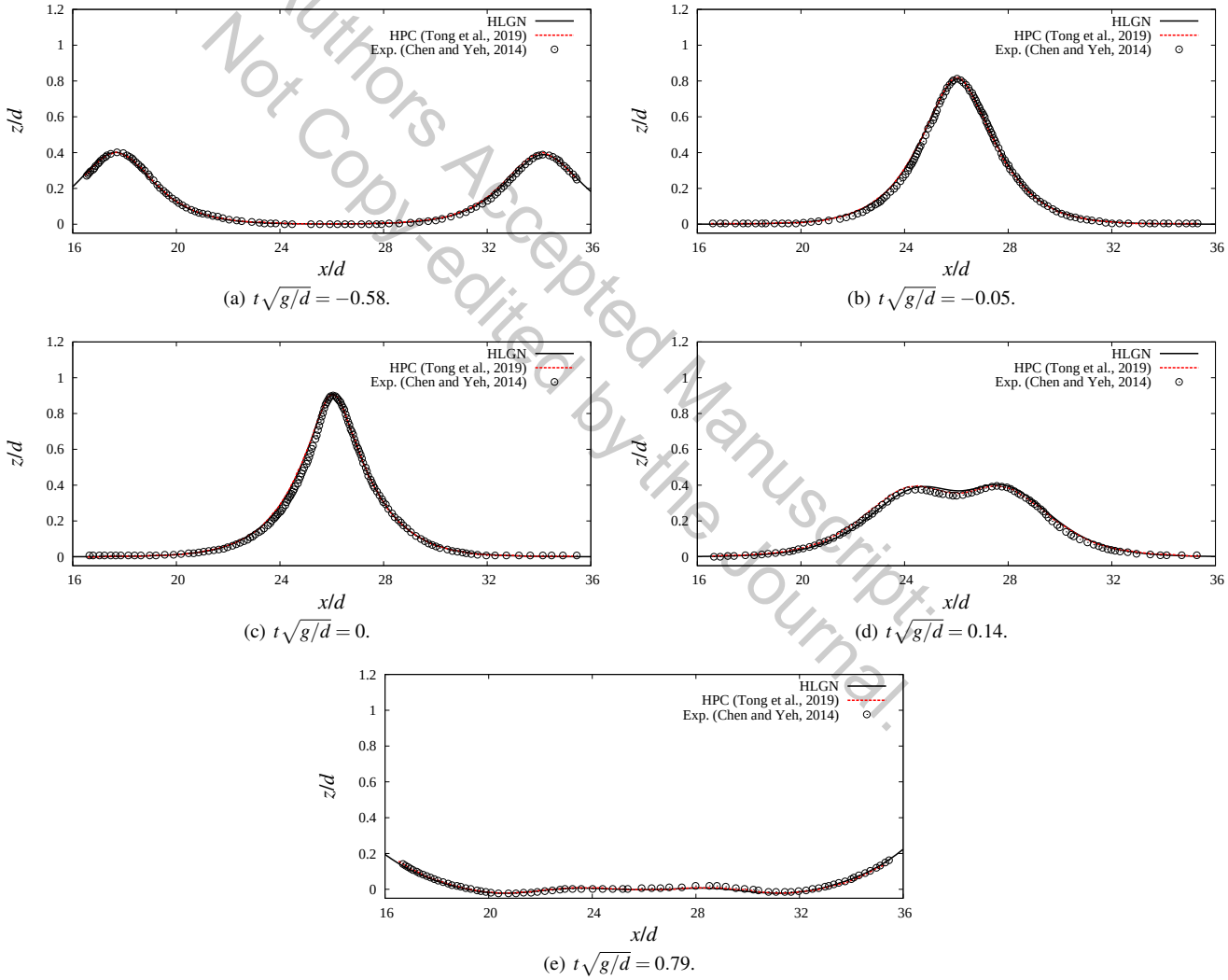

(a) $t\sqrt{g/d}=-0.58$. (b) $t\sqrt{g/d}=-0.05$.

(c) $t\sqrt{g/d}=0$. (d) $t\sqrt{g/d}=0.14$.

(e) $t\sqrt{g/d}=0.79$.

FIG. 5. Comparison between the HLGN results, HPC results and the experimental data for the surface-elevation snapshots at different times, Case 3.

wave is initially located at $x/d = 45$, and the peak of the right wave is initially located at $x/d = 120$. We set the background linear shear current everywhere outside the two solitary-wave regions. After comparing results of the HLGN model for different level K, we observe that the HLGN-5 model provides the converged results in this case as well. The computational time on Intel Core i7-8850H CPU with 2.60 GHz is about 10 minutes for simulating wave propagation for 40 seconds in these cases. The memory usage is about 20 MB.

A. Wave-surface elevation

We first focus on the wave-surface elevation during the head-on collisions. Case 7 is considered as an example, and the wave-surface elevation during the collision at different times are shown in Fig. 6, where $t\sqrt{g/d} = 0$ is the time when the maximum surface displacement occurs. Initially, the left wave, propagating in the opposite direction of the current, is wider than the right wave, propagating in the same direction as the current, as shown in Fig. 6(a). As the time passes, the two solitary waves encounter as shown in Fig. 6(b), where it is observed that the amplitudes of the waves have almost remained intact. At time $t\sqrt{g/d} = -2.21$, very close to the time when the maximum surface displacement occurs, the amplitude of solitary wave propagating to the left increases faster than the solitary wave propagating to the right, shown in Fig. 6(c). The maximum surface displacement occurs at time $t\sqrt{g/d} = 0$, shown in Fig. 6(d). It is found that the maximum surface displacement is $z/d = 0.656$, about 1.09 times larger than the sum of the two solitary-wave amplitudes, $2H/d = 0.6$. After the collision and as the solitary waves are about to pass through the point of maximum surface displacement, the solitary wave propagating to the left keeps its larger amplitude than that of the right-going solitary wave, shown in Fig. 6(e). At last, the two solitary waves separate from each other as shown in Fig. 6(f). In Fig. 6(g), we also observe some following wave trains for each solitary wave. It is observed that when the maximum surface displacement occurs, it is symmetrical for the no-current case, as shown in Fig. 7(a). While in the presence of the background linear shear current, the wave elevation becomes asymmetrical at the point of maximum displacement, as shown in Fig. 7(b). It is observed that near the peak of the wave at the point of maximum surface displacement, the two sides of the wave are on top of each other, while near the SWL, the right-side elevation is wider than the left-side elevation.

Next, the effect of the current strength on the wave elevation at the point of the maximum surface displacement is considered. The wave-surface elevations when the maximum surface displacement occurs for the current strengths $U/c_0 = 0, -0.1, -0.3$ and -0.5 (Cases 4-7) are shown in Fig. 8, where we re-center the maximum surface displacements at the same position $x/d = 0$. Near the maximum surface displacement, the wave elevation is narrower with the stronger current. While near the SWL, the wave profile is wider with increasing current velocity.

The temporal variations of the peak horizontal positions of the two solitary waves of Case 7 are shown in Fig. 9, where $t\sqrt{g/d} = 0$ is the time when the maximum surface displacement occurs. The linear fitting result is also shown in Fig. 9. It is observed that there is only one wave peak propagating from right to left for the duration T_r near $t\sqrt{g/d} = 0$. Wave speeds of the two waves increase slightly after the collision.

Next, the current effect on the phase lag time, T_r, is studied when only a single crest exists in the domain following the studies of Cooker et al.[42] and Tong et al.[36]. Results of the phase lag time in the presence of linear shear current is shown in Table IV. When $U/c_0 = -0.1$ and -0.3, the current causes larger phase lag time comparing with the no-current case.

TABLE IV. Phase lag time of the head-on collision of the two solitary waves in the presence of linear shear current.

Case	U/c_0	$T_r(g/d)^{0.5}$
4	0	3.19
5	-0.1	3.50
6	-0.3	3.51

B. Velocity field

In this section, we first present the distribution of the horizontal velocity along the water column at the maximum surface displacement followed by discussion about the two-dimensional velocity field.

Distributions of the horizontal velocity under the peak of the wave of Cases 5-7 are shown in Fig. 10, where we re-center the maximum surface displacement at $x/d = 0$. For comparison purposes, we also present the horizontal velocity of the current only. We note that for the no-current case (Case 4), the horizontal velocity along the water column at the maximum surface displacement is zero when the two solitary waves have the same amplitude (similar conclusion has been reached by Chen et al.[26]).

From Fig. 10, it is observed that the change in the current velocity significantly affects the horizontal velocity distribution. The horizontal velocity is positive (i.e. the opposite direction to the background current) near the bottom, while it is negative (i.e. the same direction to the background current) near the surface. It is also observed that at the collision point, the velocity near the surface is significantly larger than the velocity induced by the current only. The difference becomes more significant for larger current velocities.

Ratios of the horizontal velocity at the peak, u_a, and on the seafloor, u_b, for Cases 5-7 are given in Table V for when the maximum surface displacement occurs. As mentioned before, u_a/c_0 and u_b/c_0 ratios increase with larger current velocities. It is remarkable that the u_a/U and u_b/U remain approximately constant for all cases; they are about 1.40 and -0.37, respectively.

To better investigate the current strength effects, the horizontal velocity along the water column under the maximum displacement for Cases 4-7 are shown in Fig. 11(a). It is

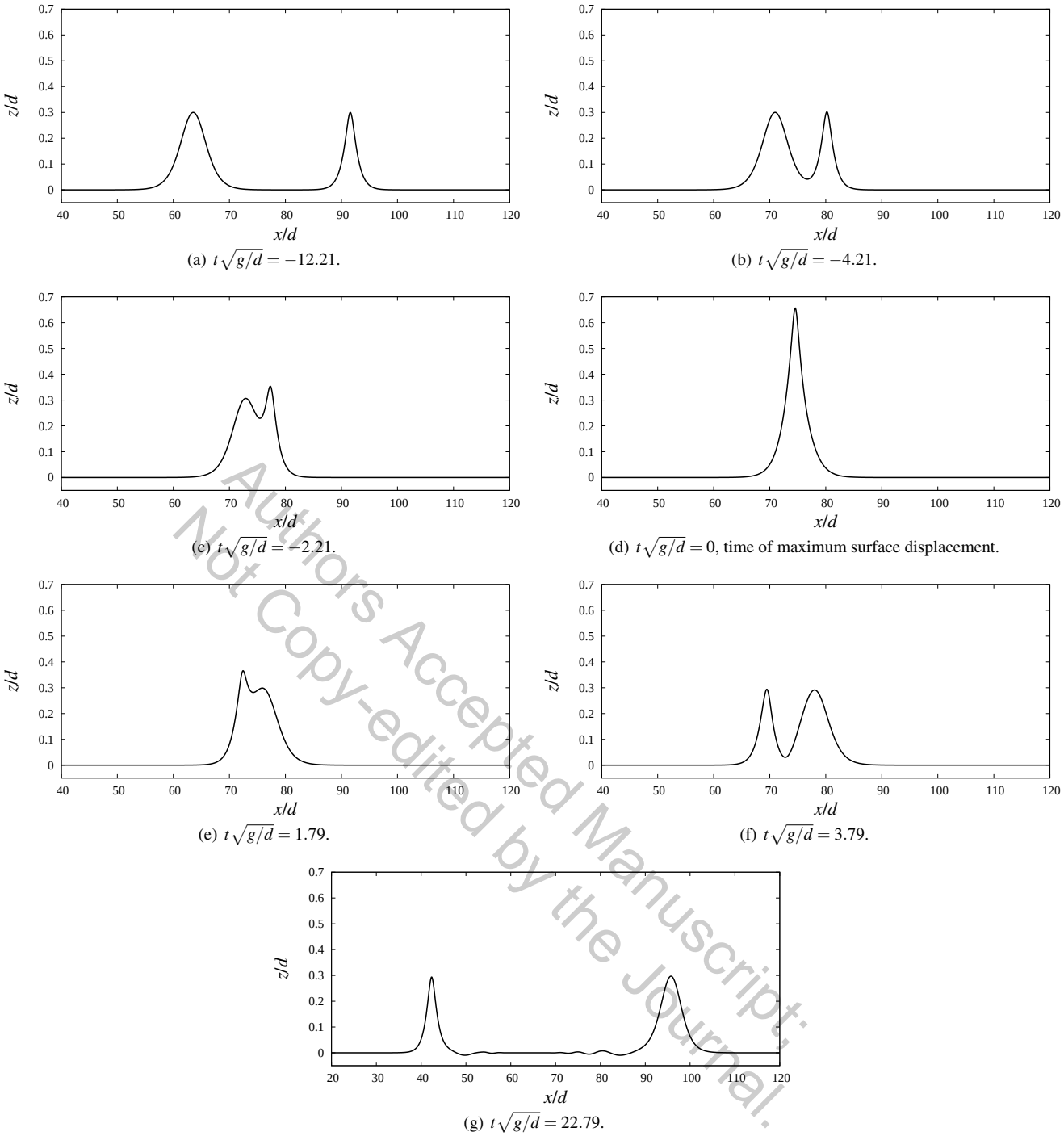

(a) $t\sqrt{g/d} = -12.21$.

(b) $t\sqrt{g/d} = -4.21$.

(c) $t\sqrt{g/d} = -2.21$.

(d) $t\sqrt{g/d} = 0$, time of maximum surface displacement.

(e) $t\sqrt{g/d} = 1.79$.

(f) $t\sqrt{g/d} = 3.79$.

(g) $t\sqrt{g/d} = 22.79$.

FIG. 6. Surface elevation during the head-on collision at different times before and after collision, $(H/d)_L = (H/d)_R = 0.3, U/c_0 = -0.5$, Case 7.

found that as the current-strength increases, both the horizontal velocities at the bottom and the free surface increase. Also, in all cases, the zero horizonal velocity occurs at almost the same depth, at about $z/d = -0.63$. Currents do not affect the position of the zero horizonal velocity. The linear superposition of the two steady solitary waves in the presence of linear shear current for Cases 4-7 is shown in Fig. 11(b). The zero linear-superposition horizontal velocity is also at almost the same depth, at about $z/d = -0.83$, which is lower than $z/d = -0.63$. The zero horizonal velocity is shifted up because of the head-on collision.

Next, we consider two moments of the head-on collision process of Case 7; namely at $t\sqrt{g/d} = -32.21$ (initial condition) and $t\sqrt{g/d} = 0$ (when the maximum surface displace-

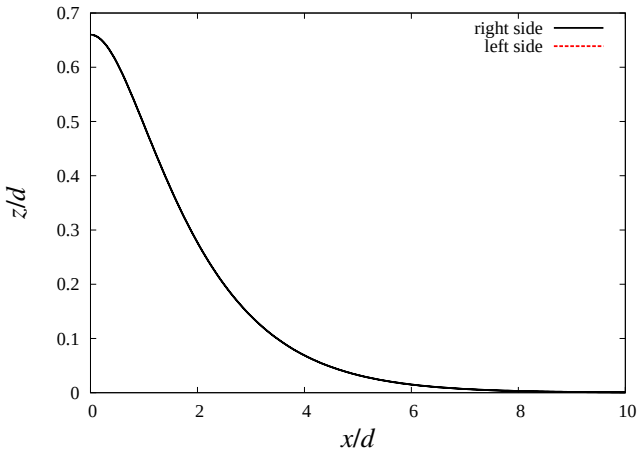

(a) $U/c_0 = 0$, Case 4.

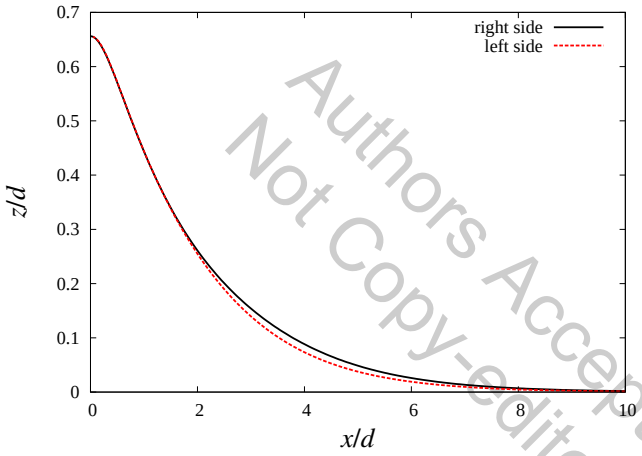

(b) $U/c_0 = -0.5$, Case 7.

FIG. 7. Comparison between the two sides of the wave surface elevation at the point of the maximum surface displacement, $(H/d)_L = (H/d)_R = 0.3$, Cases 4 and 7.

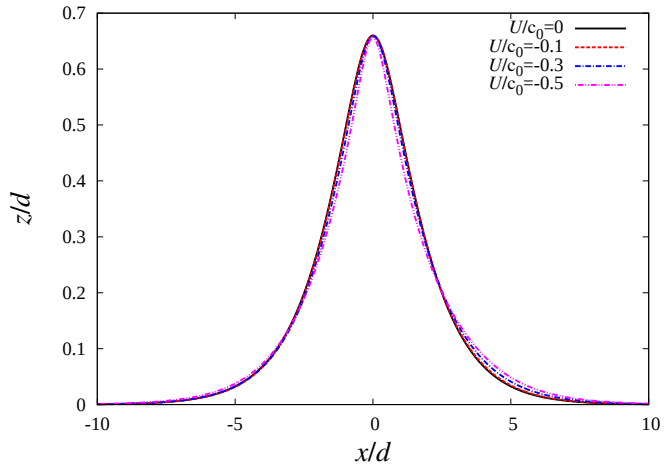

FIG. 8. Wave profile at the point of the maximum displacement for different current velocities U/c_0, $(H/d)_L = (H/d)_R = 0.3$, Cases 4-7.

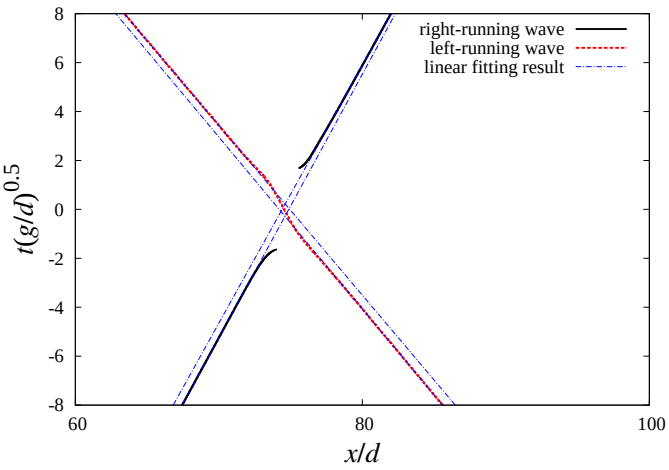

FIG. 9. Temporal variation of the peak horizontal positions of the two solitary waves, $(H/d)_L = (H/d)_R = 0.3, U/c_0 = -0.5$, Case 7.

TABLE V. Ratios of the horizontal velocity under the peak of the wave.

Case	U/c_0	u_a/c_0	u_b/c_0	u_a/U	u_b/U
5	-0.1	-0.140	0.037	1.400	-0.370
6	-0.3	-0.420	0.110	1.400	-0.367
7	-0.5	-0.707	0.184	1.414	-0.368

ment occurs). Figure 12 shows the velocity field under the two solitary waves, at $t\sqrt{g/d} = -32.21$, including the section of the left solitary wave $x/d = 30\sim60$ in Fig. 12(a) and the section of the right solitary wave $x/d = 105\sim135$ in Fig. 12(b). We observe the formation of an obvious vortex near $z/d = -0.3$ under the wave crest for the solitary wave propagating in the opposing shear current (left solitary wave), and the center of the vortex is marked with red dot as seen in Fig. 12(a). However, no such vortex is found for the solitary wave propagating in the following shear current (right solitary wave), as shown in Fig. 12(b).

The velocity field when the maximum surface displacement occurs is shown in Fig. 13(a). The red dot is used to mark the center of the vortex. Presence of a vortex is observed, although it is not as strong and clear as before. In order to see the vortex clearly, we enlarge the velocity field in Fig. 13(b). At this moment, the vertical position of the center of the vortex is at about $z/d = -0.61$, which is much lower than the initial position at about $z/d = -0.3$ shown in Fig. 12(a). It is also observed that the horizontal position of the vortex is not exactly under the maximum surface displacement. Instead, it is shifted slightly to the right side of the horizontal position of the maximum surface displacement.

C. Particle trajectory

In this subsection, we consider the particle trajectories during the collision process for Cases 4-7. To obtain the particle trajectories, we use a Lagrangian approach and keep track of

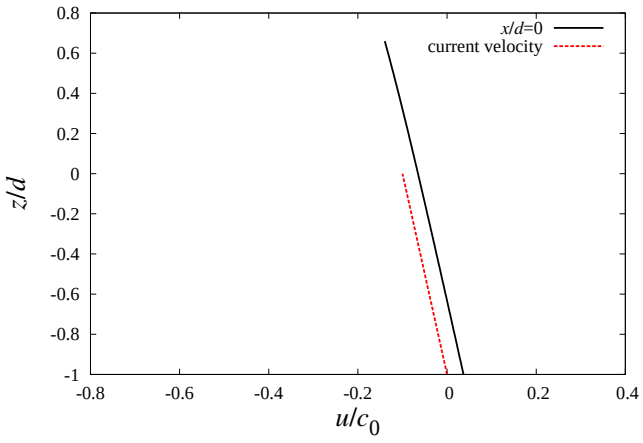

(a) $U/c_0 = -0.1$, Case 5.

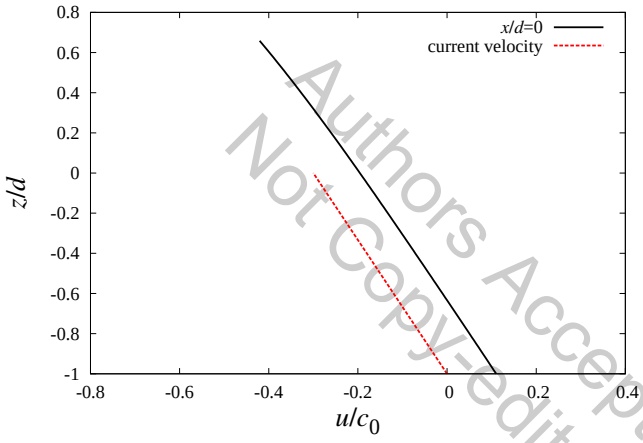

(b) $U/c_0 = -0.3$, Case 6.

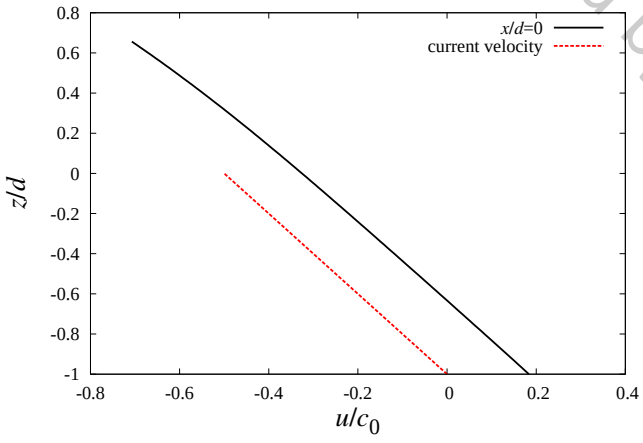

(c) $U/c_0 = -0.5$, Case 7.

FIG. 10. Horizontal velocity along the water column at the point of maximum surface displacement, $(H/d)_L = (H/d)_R = 0.3$, Cases 5-7.

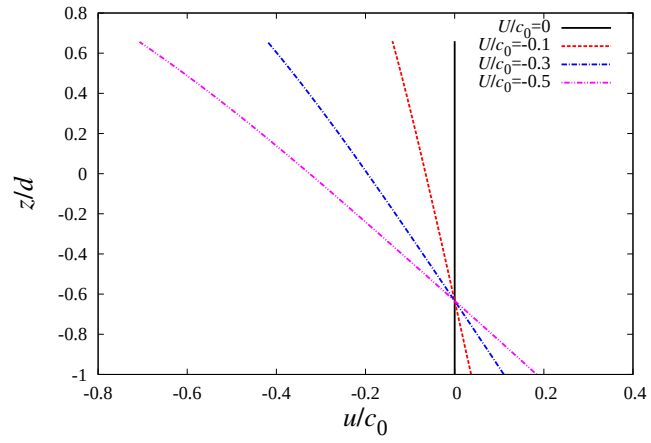

(a) Horizontal velocity along the water column under the wave crest when the maximum displacement occurs.

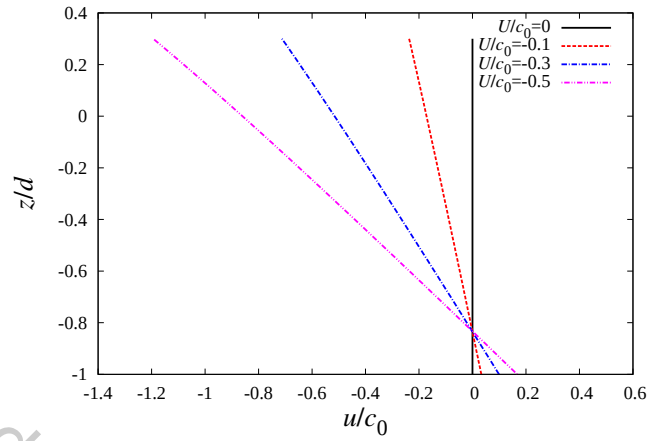

(b) Linear superposition of the two steady solitary waves in the presence of linear shear current.

FIG. 11. Comparison of distribution of the horizontal velocity, $(H/d)_L = (H/d)_R = 0.3$, Cases 4-7.

the motion of nine particles, initially located at various horizontal and vertical positions shown in Fig. 14 by the black circles. c_1 and c_2 are speeds of the right-going solitary wave and the left-going solitary wave, respectively.

We first briefly introduce the numerical method to track the particle trajectory. Suppose at initial time t_0, a given particle is at (x_0, z_0). We can obtain the new position (x_1, z_1) of the particle at time t_1 as

$$x_1 = x_0 + \int_{t_0}^{t_1} u \mathrm{d}t, \tag{11a}$$

$$z_1 = z_0 + \int_{t_0}^{t_1} w \mathrm{d}t, \tag{11b}$$

where $\mathrm{d}t$ is the time step. In this work, we select $\mathrm{d}t = 10^{-6}$s in order to track the particle trajectory accurately.

The initial locations of the particles are chosen by having a priori knowledge about the location of the maximum displacement due to the collision of the solitary waves. The mid-

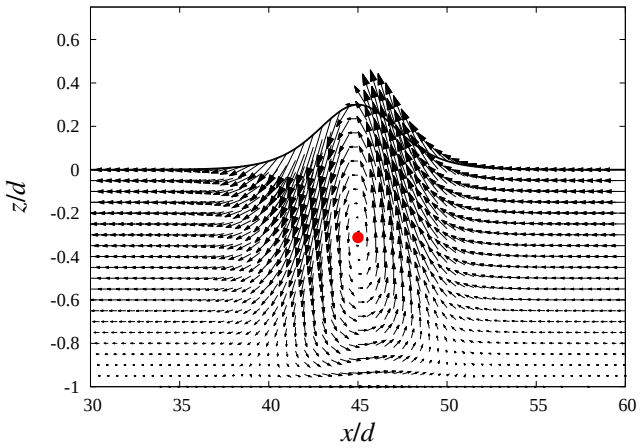

(a) Velocity field for the solitary wave propagating from left to right.

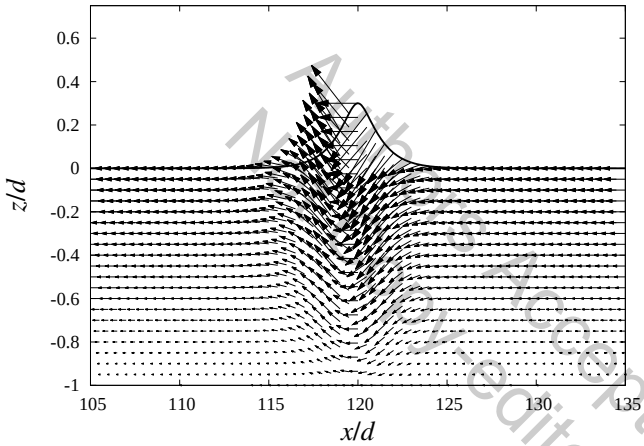

(b) Velocity field for the solitary wave propagating from right to left.

FIG. 12. Velocity field of the two solitary waves in the presence of shear current at $t\sqrt{g/d} = -32.21$, $(H/d)_L = (H/d)_R = 0.3, U/c_0 = -0.5$, Case 7.

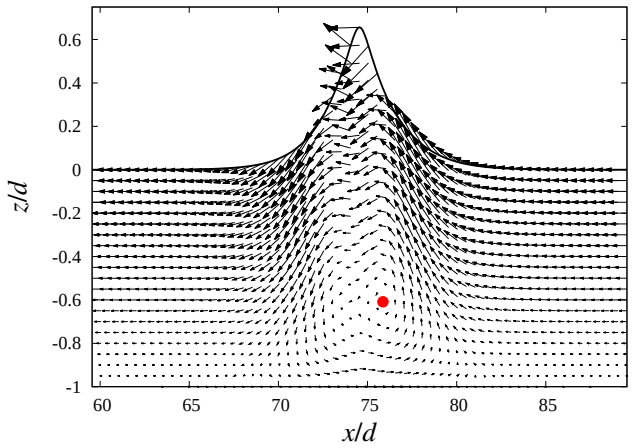

(a) Velocity field around the maximum surface displacement.

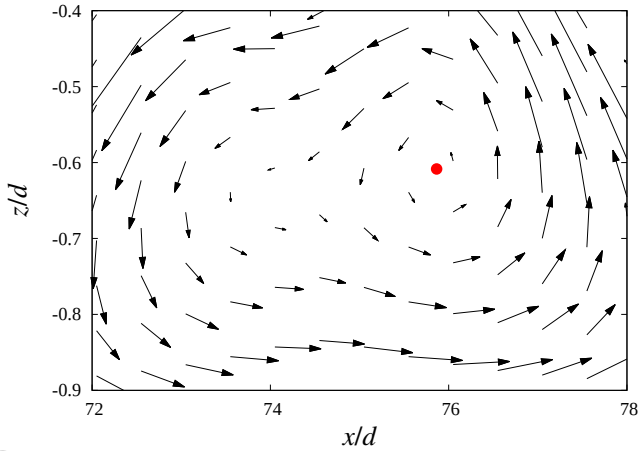

(b) Enlarged area.

FIG. 13. Velocity field under the maximum displacement point at $t\sqrt{g/d} = 0$, $(H/d)_L = (H/d)_R = 0.3, U/c_0 = -0.5$, Case 7.

dle column particles are placed at the location of the maximum displacement. The left column particles and right column particles, shown in Fig. 14, are then set at equal distances $x/d = 16$ on the left and right of the middle column particles, respectively. To capture the change in particle trajectory with depth, the particles are distributed at three rows in the vertical direction. The top row is on the SWL ($z/d = 0$), and the lower rows are at $z/d = -0.2$ and -0.5. The initial location of all nine particles are shown in Fig. 14. These particle trajectories of Cases 4-7 are shown in Fig. 15, where the black circles represent the initial particle positions.

For the no-current case (Case 4) shown in Figs. 15(a) to 15(c), it is found that all particles follow a path and eventually return approximately to their initial positions. Moreover, the trajectories of the left particles and the right particles are symmetrical for particles at the same vertical positions.

For Case 5, $U/c_0 = -0.1$, the particle trajectories are shown in Figs. 15(d) to 15(f), and obvious differences are observed when compared with the no-current case, even though the current velocity is not large. None of the particles return to their initial positions. Closed loops and motion peak are found for the left and right column particle trajectories at all three vertical positions. The left column particles first make closed-loop motions followed by phugoid motions. On the contrary, the right column particles first undergo phugoid motions followed by the closed-loop motions. No closed loops are observed for the middle column particles in this case.

The trajectories of Case 6, $U/c_0 = -0.3$, are shown in Figs. 15(g) to 15(i). With the stronger current velocity in this case, the closed loops are only observed for the trajectories of the left and the right column particles at $z/d = -0.5$. The closed-loop motion is also observed for the middle column particle at $z/d = -0.5$.

Figures. 15(j) to 15(l) show the particle trajectories of Case 7 with $U/c_0 = -0.5$, where the current strength is the strongest among all cases. The closed loops do not exist anymore and when compared with Cases 5-6, two peaks, rather than one peak, for the middle-particle trajectories at $z/d = -0.2$ is observed.

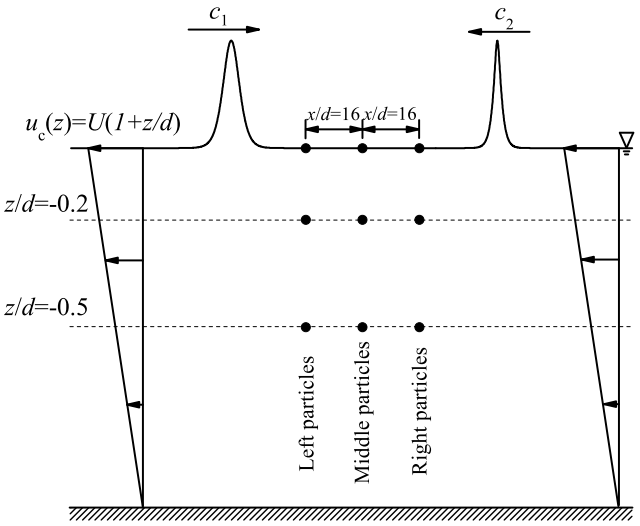

FIG. 14. Initial location of the nine particles set for the head-on collision of two solitary waves in the presence of a linear shear current. The initial location of the particles varies in different cases.

V. SUMMARY AND CONCLUSIONS

The HLGN model is developed to study the head-on collisions of solitary waves in the presence of linear shear current. Only two solitary waves with the same amplitudes are considered in this study, although this is not a requirement in general. Four conditions are considered by varying the current velocity from zero to a strong current with $U/c_0 = -0.5$.

It is understood that the head-on collision process is remarkably affected by initial conditions. To ensure suitability and accuracy of the initial conditions, results of the model are first compared with existing data of the literature for (i) a solitary wave propagating over a shearing current, and (ii) solitary-wave collision, in the absence of a background current. Excellent agreements with the laboratory measurements and other theoretical solutions are observed. The HLGN model is then used to study solitary-wave collision in the presence of a linear shear current.

It is shown that the profile of the maximum surface displacement is significantly affected by the background linear shear current. It is found that stronger current leads to a narrower wave elevation near the maximum surface displacement and a wider elevation near the SWL.

It is observed that the background shear current has a significant effect on the horizontal velocity along the water column at the point of maximum surface displacement. The direction of the horizontal velocity is opposite of the current direction near the seafloor, and following the current direction near the free surface. Stronger currents lead to larger horizontal velocities at both the bottom and free surface. Vortex is formed in the fluid field due to the propagation of a solitary wave over an opposing current. At the point of the collision and maximum surface displacement, the vertical position of the vortex is lower than that of the initial vortex, and its horizontal position is shifted upstream.

We also present the particle trajectories during the head-on collision process. It is found that the particle follows a loop motion. The loop motions become smaller with larger current velocities. At the point of the maximum surface displacement, smaller loop motions are caused by the strong current under the surface.

ACKNOWLEDGEMENT

The second author's (B.B.Z) work is supported by the National Natural Science Foundation of China (No. 11972126), the Fundamental Research Funds for the Central Universities (No. 3072022FSC0101) and the Heilongjiang Touyan Innovation Team Program.

REFERENCES

[1]D. Korteweg and G. de Vries, "On the change of form of long waves advancing in a rectangular canal, and on a new type of long stationary waves," Philosophical Magazine **39**, 422–443 (1895).
[2]D. Dutykh and D. Clamond, "Efficient computation of steady solitary gravity waves," Wave Motion **51(1)**, 86–99 (2014).
[3]B. B. Zhao, R. C. Ertekin, W. Y. Duan, and M. Hayatdavoodi, "On the steady solitary-wave solution of the Green-Naghdi equations of different levels," Wave Motion **51(8)**, 1382–1395 (2014).
[4]W. Y. Duan, Z. Wang, B. B. Zhao, R. C. Ertekin, and J. W. Kim, "Steady solution of the velocity field of steep solitary waves," Applied Ocean Research **73**, 70–79 (2018).
[5]J. K. Hunter and J.-M. Vanden-Broeck, "Accurate computations for steep solitary waves," Journal of Fluid Mechanics **136**, 63–71 (1983).
[6]Y. F. Wang and P. L.-F. Liu, "On finite amplitude solitary waves-A review and new experimental data," Physics of Fluids **34**, 101304 (2022).
[7]N. C. Freeman and R. S. Johnson, "Shallow water waves on shear flows," Journal of Fluid Mechanics **42**, 401–409 (1970).
[8]R. A. Dalrymple, "A finite amplitude wave on a linear shear current," Journal of Geophysical Research **79(30)**, 4498–4504 (1974).

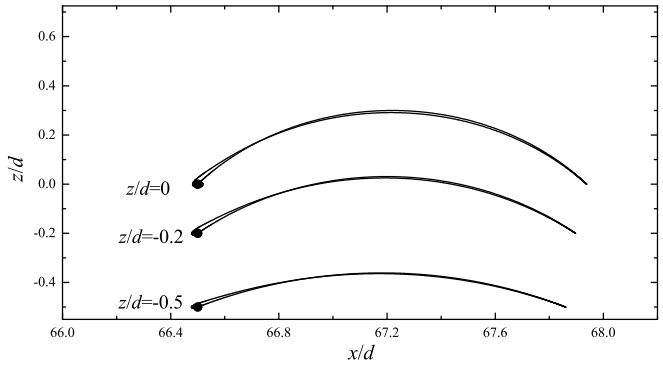

(a) Left column particle, $x/d = 66.50$, Case 4.

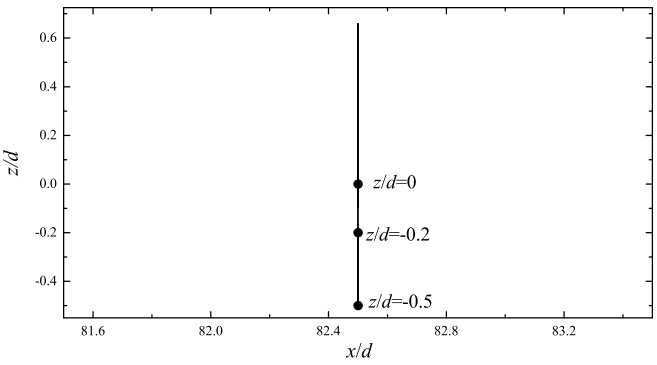

(b) Middle column particles, $x/d = 82.50$, Case 4.

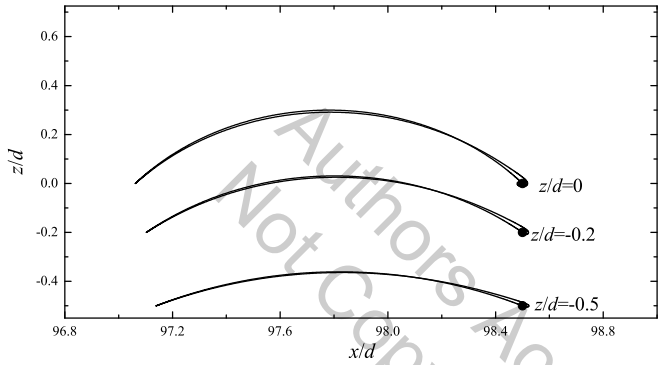

(c) Right column particles, $x/d = 98.50$, Case 4.

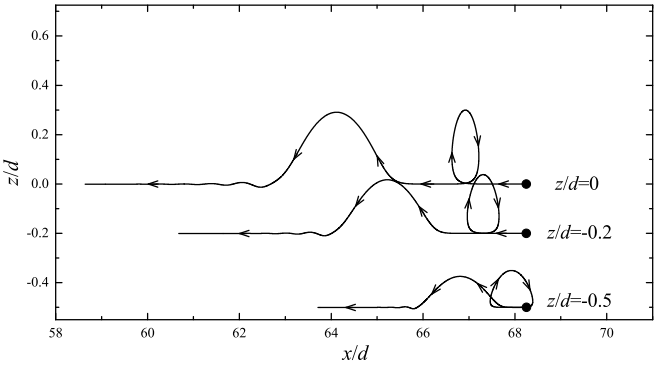

(d) Left column particles, $x/d = 68.25$, Case 5.

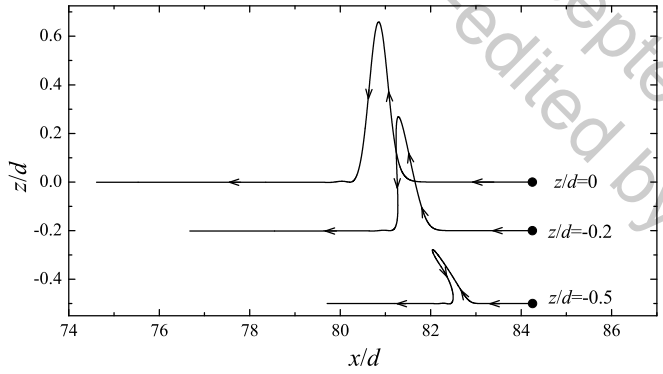

(e) Middle column particles, $x/d = 84.25$, Case 5.

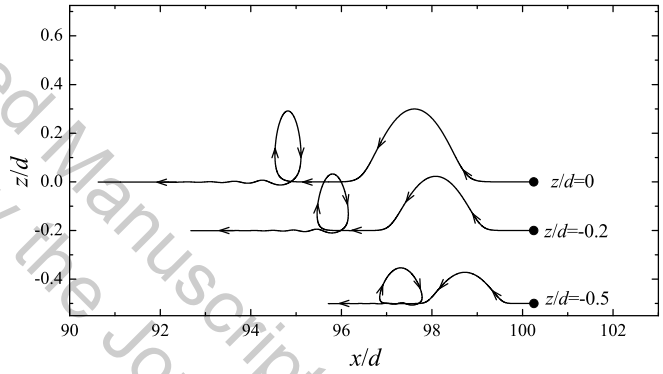

(f) Right column particles, $x/d = 100.25$, Case 5.

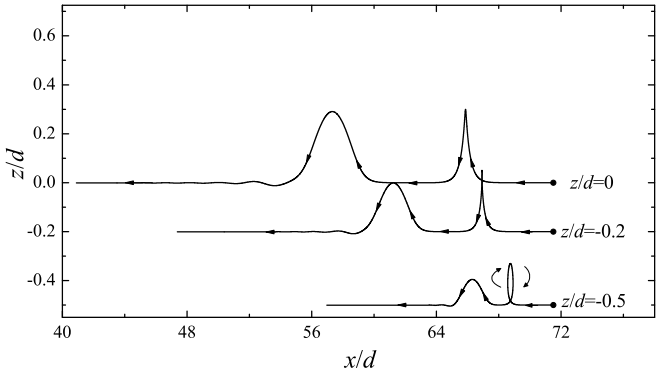

(g) Left column particles, $x/d = 71.50$, Case 6.

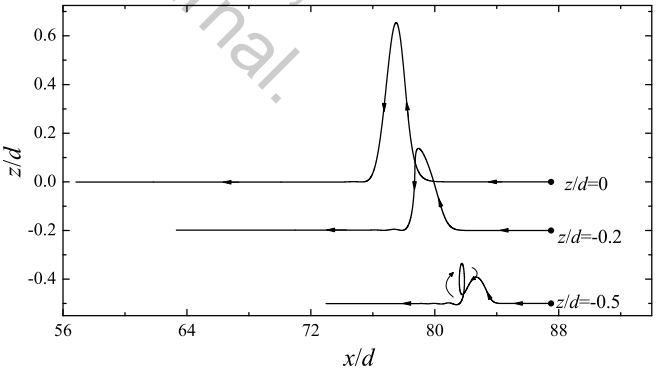

(h) Middle column particles, $x/d = 87.50$, Case 6.

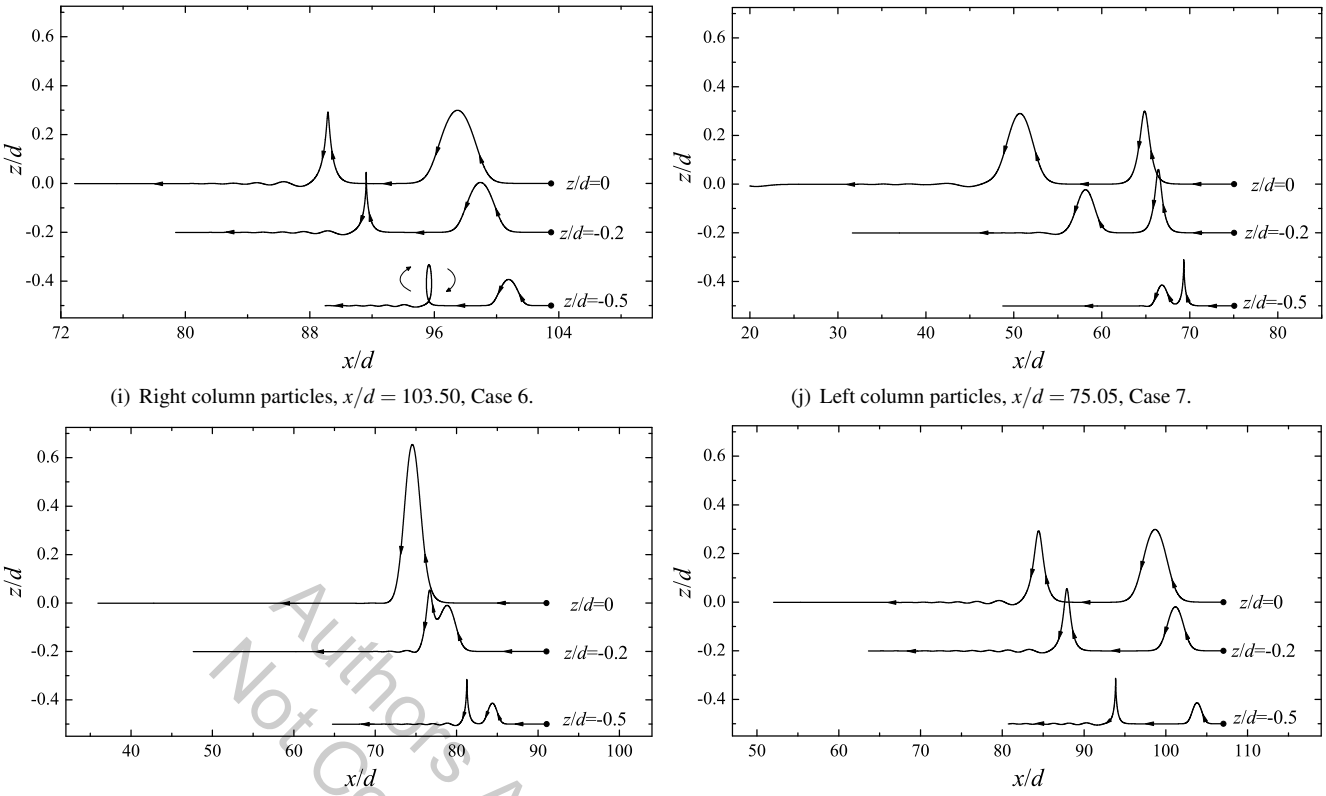

(i) Right column particles, $x/d = 103.50$, Case 6.

(j) Left column particles, $x/d = 75.05$, Case 7.

(k) Middle column particles, $x/d = 91.05$, Case 7.

(l) Right column particles, $x/d = 107.05$, Case 7.

FIG. 15. Particle trajectories of Cases 4-7, $(H/d)_L = (H/d)_R = 0.3$, see Table III for current velocities of each case.

[9] A. F. Teles Da Silva and D. H. Peregrine, "Steep, steady surface waves on water of finite depth with constant vorticity," Journal of Fluid Mechanics **195**, 281–302 (1988).
[10] C. Swan, "An experimental study of waves on a strongly sheared current profile," Proceedings of 22nd International Conference on Coastal Engineering, Delft, Netherlands, July 2-6 , 489–502 (1990).
[11] J.-M. Vanden-Broeck, "Steep solitary waves in water of finite depth with constant vorticity," Journal of Fluid Mechanics **274**, 339–348 (1994).
[12] W. Choi, "Strongly nonlinear long gravity waves in uniform shear flows," Physical Review E **68(2)**, 026305 (2003).
[13] A. Constantin, R. I. Ivanov, and E. M. Prodanov, "Nearly-Hamiltonian structure for water waves with constant vorticity," Journal of Mathematical Fluid Mechanics **10**, 224–237 (2008).
[14] O. S. Pak and K. W. Chow, "Free surface waves on shear currents with non-uniform vorticity: third-order solutions," Fluid Dynamics Research **41(3)**, 035511 (2009).
[15] P. Guyenne, "A high-order spectral method for nonlinear water waves in the presence of a linear shear current," Computers & Fluids **154**, 224–235 (2017).
[16] W. Y. Duan, Z. Wang, B. B. Zhao, R. C. Ertekin, and W. Q. Yang, "Steady solution of solitary wave and linear shear current interaction," Applied Mathematical Modelling **60**, 354–369 (2018).
[17] Z. Wang, B. B. Zhao, W. Y. Duan, R. C. Ertekin, M. Hayatdavoodi, and T. Y. Zhang, "On solitary wave in nonuniform shear currents," Journal of Hydrodynamics **32(4)**, 800–805 (2020).
[18] T. Gao, P. Milewski, and J.-M. Vanden-Broeck, "Hydroelastic solitary waves with constant vorticity," Wave Motion **85**, 84–97 (2019).
[19] S. F. Li, J. Chen, A. Z. Cao, and S. J. B., "A nonlinear Schrödinger equation for gravity waves slowly modulated by linear shear flow," Chinese Physics B **28(12)**, 124701 (2019).
[20] S. F. Li, C. C. Yu, S. H. Qian, and S. J. B., "Interfacial waves modulated by linear shear flow of the upper layer in a two-layer fluid with arbitrary layer depths," Physics of Fluids **33(4)**, 042112 (2021).
[21] S. F. Li, X. H. Xie, D. K. Chen, and S. J. B., "Modulation effect of linear shear flow on interfacial waves in a two-layer fluid with finite layer depths," Physics of Fluids **34(9)**, 092105 (2022).
[22] Z. Wang, X. Guan, and J.-M. Vanden-Broeck, "Progressive flexural-gravity waves with constant vorticity," Journal of Fluid Mechanics **905**, A12 (2020).
[23] T. Maxworthy, "Experiments on collision between solitary waves," Journal of Fluid Mechanics **76**, 177–185 (1976).
[24] J. Hammack, D. Henderson, P. Guyenne, and Y. Ming, "Solitary-wave collisions," Proceedings of 23rd International Conference on Offshore Mechanics and Arctic Engineering, OMAE 2004, Vancouver, June 21–22 (2004).
[25] Y. Chen and H. Yeh, "Laboratory experiments on counter-propagating collisions of solitary waves. Part 1. Wave interactions," Journal of Fluid Mechanics **749**, 577–596 (2014).
[26] Y. Chen, E. Zhang, and H. Yeh, "Laboratory experiments on counter-propagating collisions of solitary waves. Part 2. Flow field," Journal of Fluid Mechanics **755**, 463–484 (2014).
[27] M. Umeyama, N. Ishikawa, and R. Kobayashi, "High-resolution PIV measurements for rear-end and head-on collisions of two solitary waves," Coastal Engineering Proceedings **1(34)** (2014).
[28] M. Umeyama, "Experimental study of head-on and rear-end collisions of two unequal solitary waves," Ocean Engineering **137**, 174–192 (2017).
[29] J. G. B. Byatt-Smith, "An integral equation for unsteady surface waves and a comment on the Boussinesq equation," Journal of Fluid Mechanics **49**, 625–633 (1971).
[30] C. H. Su and R. M. Mirie, "On head-on collisions between two solitary waves," Journal of Fluid Mechanics **98**, 509–525 (1980).
[31] R. M. Mirie and C. H. Su, "Collisions between two solitary waves. Part 2. A numerical study," Journal of Fluid Mechanics **115**, 475–492 (1982).
[32] R. C. Ertekin and J. V. Wehausen, "Some soliton calculations," Proceedings of 16th Symposium on Naval Hydrodynamics, Berkeley, California, July 13–18 , 167–184 (1986).

[33]W. Craig, P. Guyenne, J. Hammack, D. Henderson, and C. Sulem, "Solitary water wave interactions," Physics of Fluids **18(5)**, 057106 (2006).
[34]J. Chambarel, C. Kharif, and J. Touboul, "Head-on collision of two solitary waves and residual falling jet formation," Nonlinear Processes in Geophysics **16(1)**, 111–122 (2009).
[35]R. C. Ertekin, M. Hayatdavoodi, and J. W. Kim, "On some solitary and cnoidal wave diffraction solutions of the Green-Naghdi equations," Applied Ocean Research **47**, 125–137 (2014).
[36]C. Tong, Y. L. Shao, F. C. W. Hanssen, Y. Li, B. Xie, and Z. L. Lin, "Numerical analysis on the generation, propagation and interaction of solitary waves by a Harmonic Polynomial Cell method," Wave Motion **88**, 34–56 (2019).
[37]Y. X. Zhang, W. Y. Duan, K. P. Liao, and S. Ma, "Numerical analysis on the effects of a submerged bottom-mounted barrier in the head-on collision of two solitary waves," Applied Ocean Research **94**, 101996 (2020).
[38]S. B. G. Karakoc, K. Omrani, and D. Sucu, "Numerical investigations of shallow water waves via generalized equal width (GEW) equation," Applied Numerical Mathematics **162**, 249–264 (2021).
[39]W. Choi, "High-order strongly nonlinear long wave approximation and solitary wave solution," Journal of Fluid Mechanics **945**, A15 (2022).
[40]M. Umeyama, "Velocity and pressure in rear-end collisions between two solitary waves with and without an underlying current," Journal of Mathematical Fluid Mechanics **21**, 37 (2019).
[41]B. B. Zhao, W. Y. Duan, and R. C. Ertekin, "Application of higher-level GN theory to some wave transformation problems," Coastal Engineering **83**, 177–189 (2014).
[42]M. J. Cooker, P. D. Weidman, and D. S. Bale, "Reflection of a high-amplitude solitary wave at a vertical wall," Journal of Fluid Mechanics **342**, 141–158 (1997).